Resonance Scattering of an Arbitrary Bessel Beam by a Spherical Object

Wei Li, *Member, IEEE*, Qiang Gui, and Zhixiong Gong, *Member, IEEE*

***Abstract*— In our prior work, multipole expansion coefficients of a Bessel beam of arbitrary order with respect to an object of arbitrary location was derived analytically and combined with the T-matrix method to numerically compute the scattering. The present work is extended to directly use the multipole expansion to calculate the scattering from an elastic spherical target. The incident Bessel beam is located at an arbitrary location with respect to the center of the sphere. The far-field resonance scattering in both on- and off-axis incidences is calculated by subtracting an appropriate background from the total scattering based on the resonance scattering theory. The results reveal that the ordinary or helicoidal Bessel beams with selected half-cone angle could lead to resonance suppression at some resonance frequencies for on-axis incidence, however, not for off-axis incidence. The intrinsic property of the elastic scattering contribution from a sphere is shown by the three-dimensional patterns of resonance scattering. The resonance scattering and suppression from thin and thick shells are also noted.**

***Index Terms*— Arbitrary order and location, Bessel beam, exact solution, multipole expansion method, resonance scattering theory (RST).**

I. Introduction

BESSEL beams have received increasing attention in optics and acoustics ever since they were proposed by Durnin [1], [2] due to the nondiffracting and self-healing properties. Particularly, the sound scattering field of a Bessel beam exhibits very different behaviors from that of ordinary plane wave incidence. The ordinary Bessel beam (OBB) has an axial peak and radially symmetric phase, while the helicoidal Bessel beams (HBBs) possess an axial null and spiral phase dislocation [3]–[8]. An ideal Bessel beam could propagate without diffraction and has infinite beamwidth, which has been resembled by a finite Bessel beam near the transducer through experimental implementations [9], [10]. The scattering of a Bessel beam from a spherical object has been derived by using the superposition of plane waves based on the partial-wave series method for the OBB [3], [4] and HBB [5]. The resonance suppression properties of the total field from an elastic spherical object centered on the axis of the Bessel beams with selected half-cone angles were investigated in detail [4]–[6]. Under certain circumstances, the canceled resonances appear due to the fact that the contribution of certain partial wave vanishes at the resonance frequency. The half-cone angle is selected to have the zero values of the Legendre polynomial for the OBB [4] or of the associated Legendre functions for HBBs [5], [6], leading to the suppression of certain resonance. Different from the plane wave incidence, the total scattering from a Bessel beam is sensitive to the beam axis with respect to the center of the object.

In the field of acoustofluidics considering vortex beams, it is interesting and necessary to investigate the scattering or related acoustic radiation force and torque exerted on an object placed in the vortex beam with arbitrary topological charge (order) and location. HBB is a type of vortex beams. A recent study extended to the off-axial Bessel beam scattering by a sphere using the spherical harmonics transform [11], [12]. A numerical quadrature was applied to calculate the expansion coefficients (also called beam-shape coefficients from the optical field) of the incident Bessel beam, which could be used to calculate the scattered field based on the scattering theory for the spherical object. Unfortunately, the formulas of the expansion coefficients are somewhat limited since the expression may be divergent when the denominator is null [11]. Under this circumstance, special attention should be paid to keep the denominator not equal to zero, which may lead to limitations of values of the dimensionless frequency. In addition, the numerical quadrature will also bring in extra calculation errors and further increase the computational cost. Hence, there is still a need to introduce the exact solution based on the multipole expansion method [8], [13] for the acoustic scattering of Bessel beams with arbitrary order and location, which is expected to overcome the limitations of the previous exact solution based on plane waves superposition and the numerical quadrature based on the spherical harmonics transform.

In this paper, another uniform and closed-form expression of acoustic scattering in an arbitrary Bessel beam are introduced by using the multipole expansion method, which could authentically improve and supplement the plane wave superposition method for the on-axial incidence case developed by Marston. Moreover, there will be no limitation on the values of the dimensionless frequency since the beam-shape coefficients are independent of the possible divergent term. It is noteworthy that a more general theory of arbitrary-order Bessel

Manuscript received November 6, 2018; accepted May 3, 2019. Date of publication May 8, 2019; date of current version August 1, 2019. This work was supported in part by the National Natural Science Foundation of China under Grant 51579112, in part by the Huazhong University of Science and Technology Postgraduate Overseas Short-Term Study Programs, and in part by China Scholarship Council under Grant 201706160043. *(Corresponding author: Zhixiong Gong.)*

The authors are with the School of Naval Architecture and Ocean Engineering, Huazhong University of Science and Technology, Wuhan 430074, China (e-mail: hustgzx@hust.edu.cn; zhixiong.gong@iemn.fr).

Digital Object Identifier 10.1109/TUFFC.2019.2915113

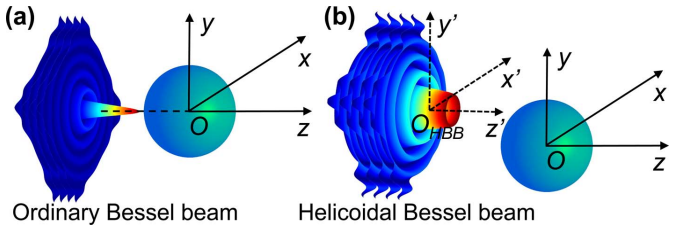

Fig. 1. Schematics of scattering from a sphere in (a) OBB with the on-axis incidence and (b) HBB with the off-axis incidence.

beam interacted with an arbitrarily located sphere has been developed for the scattering fields, powers of scattering and absorption, and axial radiation forces [14], which is outside the scope of the present work. In addition, the resonance scattering theory (RST) [15], [16] for acoustic scattering is applied to discuss the pure resonance scattering contribution from the elastic sphere and spherical shell in detail. Moreover, the on- and off-axial 3-D scattering patterns are depicted in terms of the far-field scattering form function moduli. The present work describes a fundamental study by giving a theoretical approach for acoustic scattering from a spherical shape placed in the arbitrary location of Bessel beams with verifications of the previous works and several new discussions.

II. Incident Coefficients Based on Multipole Expansion Method

In this section, the spherical targets placed in the nonviscous and homogeneous fluid are considered to investigate the scattering of a Bessel beam with the on-axis and off-axis incidences, as shown in Fig. 1(a) for an OBB and (b) for an HBB. Taking an ideal Bessel beam with arbitrary order and location as an example [Fig. 1(b)], the incident potential field of a Bessel beam with the arbitrary origin O_{HBB} located in (x_0, y_0, z_0) in the xyzO coordinate system could be expressed as

$$\Phi_{\mathrm{ABB}} = \Phi_0 e^{-i\omega t} i^M e^{ik_z(z-z_0)} J_M(k_r R') e^{iM\varphi'} \tag{1}$$

where Φ_0 denotes the beam amplitude, M is the topological charge of the beam with $M = 0$ corresponding to OBB, and $M \geq 1$ corresponding to HBBs. J_M is the cylindrical Bessel function of the indicated argument, $k_z = k\cos\beta$ and $k_r = k\sin\beta$ are the respective axial and radial wavenumbers. In the off-axis incidence, the projection of radial distance for an arbitrary field point (x, y, z) in $x'O_{\mathrm{HBB}}y'$ is $R' = ((x-x_0)^2 + (y-y_0)^2)^{1/2}$, and the corresponding azimuthal angle $\varphi' = \tan^{-1}[(y-y_0)/(x-x_0)]$. Since all the fields have the same time dependence, the time-harmonic factor $e^{-i\omega t}$ is suppressed in the following throughout. The main idea of the multipole expansion method [8], [13] is to use the well-known spherical harmonics expansion [17]. Hence, (1) could be rewritten as the product form of the incident expansion coefficients a_{nm} and basis wave functions

$$\Phi_{\mathrm{ABB}} = \Phi_0 \sum_{n=0}^{\infty} \sum_{m=-n}^{n} i^n a_{nm} \times j_n(kr) Y_{nm}(\theta, \varphi) \tag{2}$$

where $j_n(kr)$ and $Y_{nm}(\theta, \varphi)$ are the spherical Bessel function of the first kind and the normalized spherical harmonic functions ($Y_{nm} = \xi_{nm} P_n^m(\cos\theta) e^{im\varphi}$ with $\xi_{nm} = ([(2n+1)(n-m)!]/[4\pi(n+m)!])^{1/2}$, respectively. The expansion coefficients of incidence a_{nm} are determined by

$$a_{nm} = \frac{1}{\Phi_0 j_n(kr)} \int_{\varphi=0}^{2\pi} \int_{\theta=0}^{\pi} \Phi_{\mathrm{ABB}} Y_{nm}^*(\theta, \varphi) \sin\theta d\theta d\varphi \tag{3}$$

where the asterisk indicates the complex conjugate of indicated expression. The expansion coefficients of the incident Bessel beams with arbitrary location and order could be obtained by using the addition theorem of cylindrical Bessel function and the exact integration of the hybrid product of the associated Legendre, cylindrical Bessel, and exponential functions in spherical coordinates [8]

$$a_{nm} = 4\pi \xi_{nm} i^{M-m} P_n^m(\cos\beta) e^{-ik_z z_0} J_{m-M}(\sigma_0) e^{-i(m-M)\varphi_0} \tag{4}$$

where $\sigma_0 = k_r R_0$ with the projection of the center of the Bessel beam (x_0, y_0, z_0) on the xOy plane, $R_0 = (x_0^2 + y_0^2)^{1/2}$, and the azimuthal angle $\varphi_0 = \tan^{-1}(y_0/x_0)$. $P_n^m(\cos\beta)$ are the associated Legendre functions with the argument related to the beam cone angle β. Note that when $m = 0$, $P_n(\cos\beta)$ specifies the Legendre polynomial. The incident coefficients in (4) depend on the azimuthal index m since the azimuthal symmetry of the Bessel beam with respect to the sphere breaks down for the off-axis illumination. The theoretical derivation of the expansion coefficients in (4) has no limitation on the dimensionless frequency since the term $j_n(kr)$ in the denominator of (3) is canceled during the procedure. When the centers of the sphere and Bessel beam coincide ($R_0 = 0$), (4) could be degraded into the on-axis expression of beam-shape coefficients [3]–[7]. After deducing the incident beam-shape coefficients a_{nm}, it is accessible to obtain the scattered potential Φ_s caused by the presence of a spherical object on the propagation path of the wave field according to the scattering theory

$$\Phi_s = \Phi_0 \sum_{n=0}^{\infty} \sum_{m=-n}^{n} i^n a_{nm} A_n h_n^{(1)}(kr) Y_{nm}(\theta, \varphi) \tag{5}$$

where A_n denotes the partial-wave coefficients of the scattered field and $h_n^{(1)}(kr)$ is the spherical Hankel function of the first kind. The partial-wave coefficients A_n could be obtained from the scattering coefficients s_n through a typical relationship $A_n = (s_n - 1)/2$. The scattering coefficients s_n of a wide variety of spherical shapes are briefly reviewed in [3], which depend on the dimensionless frequency ka, the boundary condition, and material properties. By the law of energy conservation, the modulus of the scattering coefficients meets $|s_n| = 1$ without absorption [18]. It is helpful to note the consistency between the T-matrix method [19], [20] and the partial wave series solution for the relationship between the partial-wave coefficients and scattering coefficients. In the T-matrix method, the transition matrix $T_{nm,n'm'}$ (similar as the partial-wave coefficients A_n in the series solution) has the form $T_{nm,n'm'} = (S_{nm,n'm'} - 1)/2$ with $S_{nm,n'm'}$ being the scattering coefficients ($|S_{nm,n'm'}| = 1$ in the absence of absorption). Both A_n and

$T_{nm,n'm'}$ give a linear relationship between the incident and scattered beam-shape coefficients. For the spherical shape with the azimuthal symmetry, the scattering coefficients are independent of the azimuthal index m, thus only depend on the partial-wave index n. This could be seen through the scattering coefficients s_n in the series solution and the simplified transition matrix $T_{nn'}$ in the T-matrix method [20]. The T-matrix method is regarded as the matrix form for all the expanded coefficients and the T matrix, while the partial series method as the series summation of different partial waves (both the terminologies of the methods are named after the characteristics). The matrix multiplication of the T matrix and incident coefficients will induce the summation of the corresponding partial waves as in a direct way in the partial-wave series.

In general, when investigations are focused on the far-field region ($kr \rightarrow \infty$), it should be noted that the spherical Hankel function of the first kind can be replaced by an asymptotic approximation $h_n^{(1)}(kr) \simeq i^{-(n+1)}e^{ikr}/(kr)$. Accordingly, the steady-state (time-independent) scattered potential in far-field could be represented in the term of form function as [21]–[23]

$$\Phi_s = \Phi_0 \frac{r_0}{2r} f(ka, \theta, \beta, \varphi) e^{ikr} \tag{6}$$

where θ is the scattering polar angle, r_0 is the characteristic length of the object, and for a spherical shape, $r_0 = a$. The far-field form function is, therefore, defined by the exact partial series as

$$f(ka, \theta, \beta, \varphi) = \frac{-2i}{ka} \sum_{n=0}^{\infty} \sum_{m=-n}^{n} a_{nm} A_n Y_{nm}(\theta, \varphi) \tag{7}$$

which could be used to compute the scattering field for the spherical shapes with different boundary conditions and material compositions, such as soft, rigid, and elastic spheres.

III. Resonance Scattering Theory for a Spherical Shape

The RST is considered to isolate the resonance scattering contribution from the total scattering field by subtracting an appropriate background. For the elastic spherical shapes, the incident wave could propagate both outside and inside the object. The impenetrable waves outside the object mainly include the contributions from the wave around the geometry (Franz wave) and rigid reflections, whereas the penetrable waves inside the object mainly consist of Rayleigh waves and Whispering Galley waves for a solid sphere and lamb waves for an empty shell. The RST is to separate each individual normal mode contribution to the overall scattering fields into two distinct parts: the resonance scattering and the nonresonance part (background). In early studies, the RST [15] has been successfully demonstrated that the rigid background is suitable for solids [16], [24] and thick shells [25], and the soft background for very thin shells [26]. Note that for a spherical shell between the thin and thick shells, the intermediate (hybrid) background may be applied to separate the resonance contribution [27], [28]. It is interesting to note that advanced background theories for multilayered cylinders have been developed recently [29], [30]. According to (7), the resonance form function can be expressed by subtracting a rigid or soft background linearly from the total scattering field as follows:

$$f^{\text{res}}(ka, \theta, \beta, \varphi) = \frac{-2i}{ka} \sum_{n=0}^{\infty} \sum_{m=-n}^{n} a_{nm} \left[A_n(ka) - A_n^{r,s}(ka) \right] Y_{nm}(\theta, \varphi) \tag{8}$$

where the partial-wave coefficients of the background $A_n^{r,s}(ka)$ could be obtained with the known scattering coefficients $s_n^r(ka) = -h_n^{(2)}(ka)/h_n^{(1)}(ka)$ for the rigid and $s_n^s(ka) = -h_n^{(2)}(ka)/h_n^{(1)}(ka)$ for the soft background terms, respectively. It is noteworthy that the form functions are complex number by (7) and the scattered fields are often described by the modulus of the form function. The resonance scattering contributions by (8) should be calculated by subtracting the complex form function of the background from that of the total scattered field and, finally, taking the modulus values of the complex resonance form function.

IV. Scattering From a Solid Sphere in an Ordinary Bessel Beam

The resonance form function presented in Section III is applied to compute the scattering of the illumination of the zeroth-order OBB by a tungsten carbide (WC) sphere submerged in water for both on- and off-axis incidences. The material for the solid sphere is selected to obtain the narrow resonances over a wide range of ka due to the weak radiation damping for the hard dense material [4]. The properties of the WC (tungsten carbide) sphere are the density $\rho_s = 13.8$ g/cm^3, the longitudinal velocity of sound $c_L = 6650$ m/s, and transverse velocity $c_T = 3981$ m/s. The density of the surrounding water is $\rho_w = 1$ g/cm^3, and the sound velocity $c_w = 1482.5$ m/s. The backscattering form functions are considered for the WC sphere in OBB by depicting the 2-D form function modulus curve versus the dimensionless frequency ka. For a solid sphere, the rigid background is appropriate for the separation of the resonance contribution from the total field. First, the RST is applied to compute the form function moduli of the background, total, and resonance scattering, respectively. Both the plane wave incidence (half-cone angle vanishes such that $\beta = 0°$) and the ordinate Bessel beams with selected half-cone angles are considered. To verify the effectiveness of the present analytical method, the on-axis incidence is studied here with several half-cone angles that make the Legendre polynomial null [$P_n(\cos\beta) = 0$]. The explicit values of the half-cone angles are listed in Table I.

Fig. 2(a)–(c) depicts the backscattering form functions of the background, total, and resonance contributions versus the dimensionless frequency ka of a WC sphere centered on the axis of OBB in water. The half-cone angles are given in each panel. As shown in Fig. 2(a), the form function moduli are slightly oscillating around $|f| = 1$ both for the plane wave and Bessel beam incidences in the geometrical region of frequency (generally, $ka > 10$). This could be explained by the *geometric optics limit* that the specular reflection modulus is independent of the scattering angle [31], [32], leading

TABLE I

SELECTED HALF-CONE ANGLES β FOR ROOTS OF LEGENDRE POLYNOMIAL $P_n(\cos\beta)=0$ AND ASSOCIATED LEGENDRE FUNCTIONS $P_n^{1,2}(\cos\beta)=0$

Bessel beams	$P_n^m(\cos\beta)=0$		β
	n	m	
OBB	2	0	54.7346°
	3	0	39.2315°
	4	0	30.5556°
	5	0	25.0173°
FHBB	3	1	63.4349°
	4	1	49.1066°
	5	1	40.0881°
SHBB	4	2	67.7923°
	5	2	54.7356°
	6	2	75.4892°

to the similar phenomenon in the backscattering even for Bessel beam whose wave vector has a cone angle relative to the beam axis. The total scattering of the WC sphere is shown in Fig. 2(b) with similar behavior as that of the rigid background in an approximate region $ka < 6$, which is due to the fact that the impenetrable waves dominate in the total scattering in this case. The oscillations come from the interferences between the specular contribution and Franz wave. The difference of the form function moduli between (a) and (b) for the first peak at approximately $ka = 1.45$ is due to the resonance of the dipole mode, as further proven in Fig. 2(c). The computational results of the scattering in Fig. 2 through the theoretical approach based on the multipole expansion method agree well with those using the T-matrix method [33] which only considered the on-axis incidence.

The resonance scattering form function [Fig. 2(c)] is acquired by subtracting the background [Fig. 2(a)] from the total scattering [Fig. 2(b)] by the RST, which shows obvious narrow resonance peaks, especially for the second to fifth-order Rayleigh resonance at $ka = 7.06$, 10.46, 13.38, and 16.10, respectively. The peaks with lower amplitudes of form function modulus and narrower resonances than those of the Rayleigh types are the Whisper Gallery types, which will not be further discussed in the present work. The canceled resonances appear for a certain resonance with an OBB with a selected half-cone angle, such that $\beta_2 = 54.7346°$ for the second-order Rayleigh resonance (R_2), $\beta_3 = 39.2315°$ for the third order (R_3), $\beta_4 = 30.5556°$ for the fourth order (R_4), and $\beta_5 = 25.0173°$ for the fifth order (R_5), as shown clearly in Fig. 2(c). The physical mechanism of the resonance suppressions in OBB was given by Marston to use the expression for the form function of a sphere based on plane wave superposition for the on-axis incidence [3], [4]

$$F(ka,\cos\theta,\cos\beta) = \frac{-i}{ka}\sum_{n=0}^{\infty}(2n+1)(s_n-1)P_n(\cos\theta)P_n(\cos\beta) \quad (9)$$

which depends on the term of Legendre polynomial $P_n(\cos\beta)$. Except for $\beta = 0°$, the other four half-cone angles β_n correspond to the respective roots of $P_n(\cos\beta)=0$ for $n = 2, 3, 4$, and 5 (see Table I with $m = 0$). The corresponding suppression

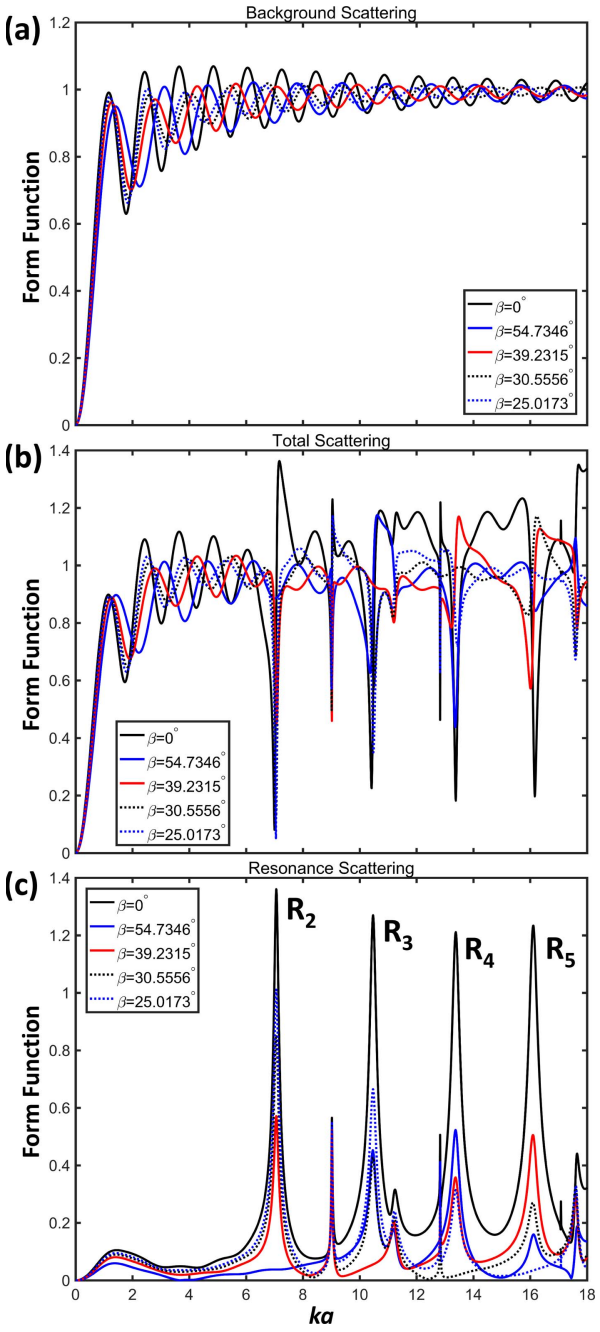

Fig. 2. (a) Rigid backscattering form function, (b) total backscattering form function, (c) pure resonance backscattering form function moduli versus the dimensionless frequency ka for a WC (tungsten carbide) sphere in water illuminated by the zeroth-order OBB with selected half-cone angles. $\beta = 0°$ specifies the plane wave limit.

of the individual Rayleigh resonance could make clear that the partial wave is suppressed with $P_n(\cos\beta_n)=0$, resulting in the partial-waveform function $F_n(ka,\cos\theta,\cos\beta_n) = 0$. However, the on-axis expression of the form function may be not able to explain the resonance phenomena for the off-axis incidence.

Note that the present expressions of (4), (7), and (8) may not be able to give the explanation of the resonance suppression in a direct way since the form function of arbitrary-order Bessel beam with the term $P_n^m(\cos\beta)$ is computed by the

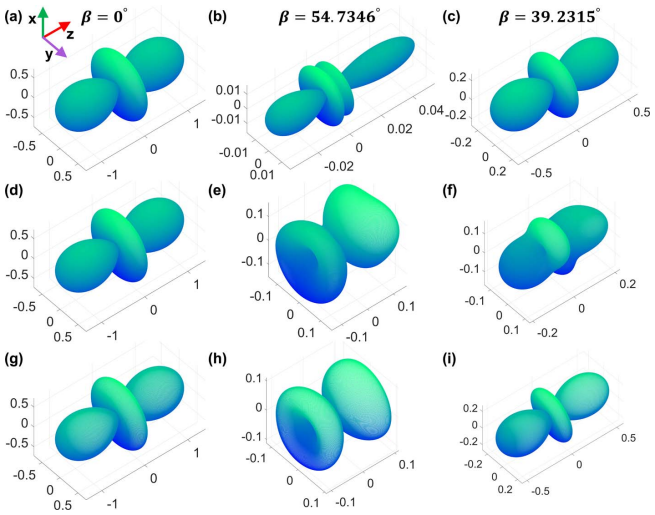

Fig. 3. 3-D resonance scattering patterns of an OBB for a WC sphere in the far field with different half-conical angles at the frequency of the second-order Rayleigh resonance $ka = 7.06$. (a) Incident direction is along the positive z-axis. The first row (a-c) is for the on-axis incidence while the second (d-f) and third (g-i) are for the off-axis with offsets $(x_0, y_0) = (\pi/ka, 2\pi/ka)$ for panels (d) and (e) and $(x_0, y_0) = (0.1\pi/ka, 0.2\pi/ka)$ for (g)–(i).

summation over all the partial-wave index n and the azimuthal index m, with $n = [0, N_{\max}]$ and $m = [-n, n]$. $N_{\max}$ is the truncation number to make the exact results convergent. However, the present work shows an *analytical method* for the scattering of the Bessel beam both on the axis $(x_0, y_0, z_0) = (0, 0, 0)$ of the object and off the axis. To further discuss the resonance scattering properties of the WC sphere in the OBB with arbitrary location, the 3-D resonance patterns of form function moduli are calculated by subtracting the rigid background at the frequency of the second-order Rayleigh resonance ($ka = 7.06$) in Fig. 3. The incidence direction is along the z-axis, as shown with the coordinates system in Fig. 3(a). The first row depicts the scattering for the on-axis incidence, while the second and third rows for the off-axis with the offsets $(x_0, y_0) = (\pi/ka, 2\pi/ka)$ and $(x_0, y_0) = (0.1\pi/ka, 0.2\pi/ka)$. Note that the offset gives a shifting distance (relative to the sphere radius) of the beam axis with respect to the center of the sphere. The half-cone angles are given on the top of each column. It could be found for the plane wave illumination [Fig. 3(a), (d), and (g)], the 3-D scattering patterns are the same since there is no difference of the incident waves between on-axis and off-axis incidences. However, the 3-D patterns for the on-axis incidence are different from those for off-axis incidence in the OBB, namely, the 3-D patterns are not axisymmetric for the off-axis of the OBB [Fig. 3(e), (f), (h), and (i)], while are still axisymmetric for the on-axis cases [Fig. 3(b) and (c)]. The offset affects the scattering patterns as shown in the second and third rows, which in fact will change the beam shape coefficients in (4). It should be noted that the scattering of the background and total field is not axisymmetric under the off-axis illumination of the OBB. Furthermore, as depicted in Fig. 3(b), the form function modulus of the R_2 resonance scattering at $ka = 7.06$ from the OBB with a half-cone angle $\beta_2 = 54.7346°$ (such that $P_2(\cos\beta_2) = 0$) is reduced significantly for the on-axis case at the frequency of R_2, which is due to the resonance suppression of the corresponding order. However, the suppression seems to be not obvious for off-axis incidence at $ka = 7.06$ with $\beta_2 = 54.7346°$ [Fig. 3(e) and (h)]. The second Rayleigh resonance should have the quadrupole mode [24], which is verified by Fig. 3(a) for the plane wave and Fig. 3(c) for the OBB without resonance suppression. It is noticeable that the 2-D polar patterns of the first five orders of Rayleigh resonances of a WC sphere were given using the T-matrix method [33], which further demonstrates the correctness of the Rayleigh resonances and the effectiveness of the present theoretical method.

V. Scattering From a Solid Sphere in a Helicoidal Bessel Beam

HBBs have the axial null of the amplitude and the spiral phase dislocation, which is different from the OBB. The incident wave is not axisymmetric because of the dependence of the azimuthal angle. The form function of the first-order HBB (FHBB) could be expressed as [5]

$$F(ka, \cos\theta, \cos\beta, \varphi) = \frac{-i}{ka} \times \sum_{n=1}^{\infty} \frac{(2n+1)}{n(n+1)} (s_n - 1) P_n^1(\cos\theta) P_n^1(\cos\beta) e^{i\varphi} \quad (10)$$

where P_n^1 is the associated Legendre function of the indicated argument. It could be observed from (10) that the scattering form functions depend on the azimuthal angle φ. The HBB is not existent for the half-cone angle $\beta = 0°$ since the term $J_M(k_r R')$ with $M \geq 1$ will vanish with $k_r = k \sin\beta = 0$. It is different that the OBB ($M = 0$) with $\beta = 0°$ gives the ordinary plane waves. For the FHBB of the on-axis incidence, the backscattering and forward scattering will vanish since $P_n^1(\cos\theta) = 0$ when the scattering angle $\theta = 180°$ or $\theta = 0°$, as observed in (10). Hence, the form function moduli of the resonance scattering of the FHBB are calculated in the direction of $\theta = 149.444°$. Different half-cone angles are selected and the 2-D form function modulus curves versus ka are given in Fig. 4(a) with the half-cone angles for roots of $P_n(\cos\beta) = 0$ and in Fig. 4(b) with β for roots of $P_n^1(\cos\beta) = 0$. The resonance peaks occur at the same frequencies as those of Fig. 2(c). There is no resonance suppression for the selected half-cone angles in Fig. 4(a) since the scattering of the FHBB depends on the term of $P_n^1(\cos\beta) = 0$ instead of $P_n(\cos\beta) = 0$ according to (10). This could be further demonstrated by Fig. 4(b) since the canceled resonances appear when β is selected for the root of the associated Legendre function $P_n^1(\cos\beta) = 0$, which are listed in Table I. The half-cone angles $\beta = 63.4349°$, $49.1066°$, and $40.0881°$ correspond to the roots of $P_n^1(\cos\beta) = 0$ for $n = 3$, 4, and 5, respectively. The resonance frequencies of the third to fifth Rayleigh resonance are $ka = 10.46$, 13.38, and 16.10, where the corresponding resonance suppression occurs with a selected β to make $P_n^1(\cos\beta)$ vanish. For the on-axis incidence in the second-order HBB (SHBB), the selected half-cone angles for the roots of $P_n^2(\cos\beta) = 0$ (see Table I) will suppress the corresponding resonance, as shown in Fig. 5.

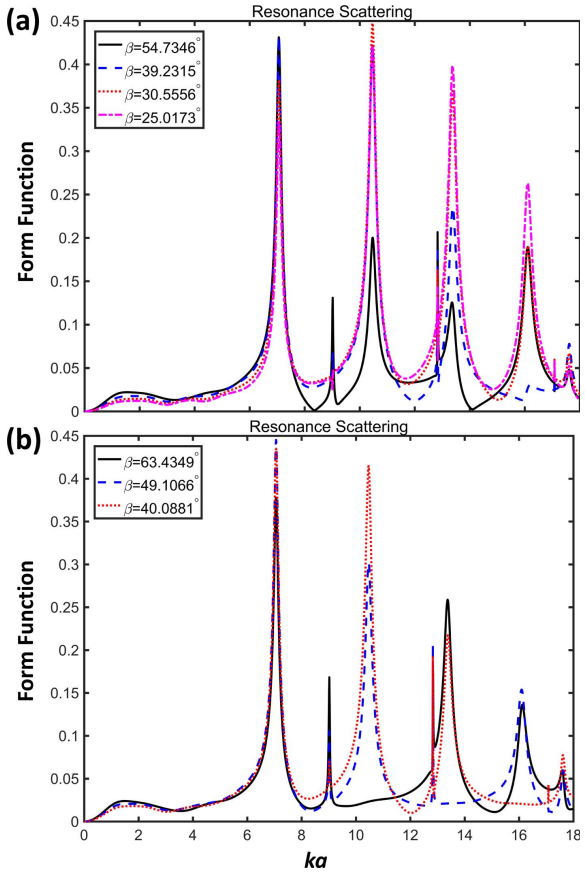

Fig. 4. Resonance scattering of the FHBB at the scattering direction $\theta = 149.444°$ versus ka with the half-cone angles β selected for roots of (a) $P_n(\cos\beta) = 0$ and (b) $P_n^1(\cos\beta) = 0$.

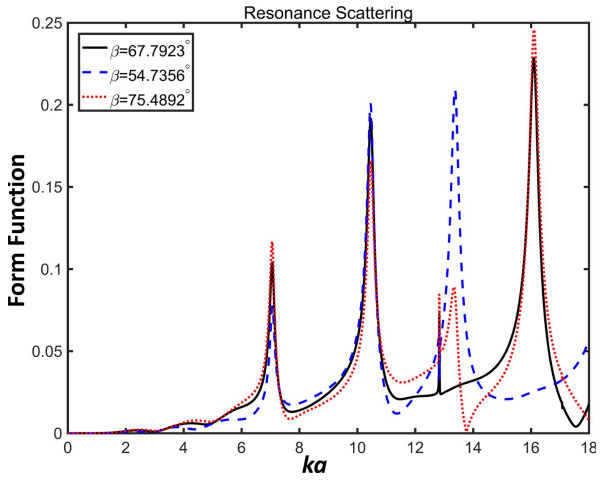

Fig. 5. Same as Fig. 4(b), except for an SHBB with β selected for roots of $P_n^2(\cos\beta) = 0$.

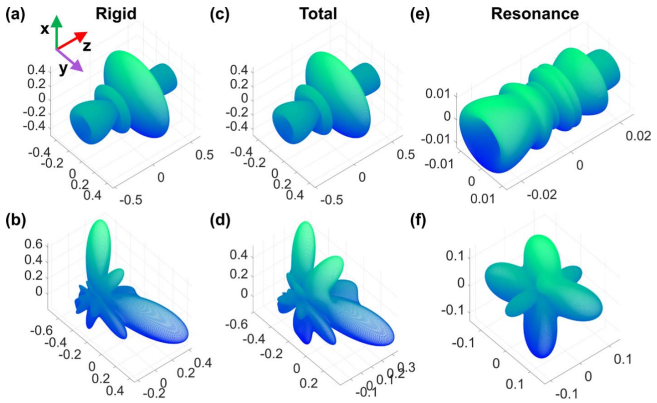

Fig. 6. 3-D resonance scattering patterns of an FHBB for a WC sphere in the far-field with $\beta = 63.4349°$ such that $P_3^1(\cos\beta) = 0$ at the frequency of the third-order Rayleigh resonance $ka = 10.46$. (a) Incident direction is along the positive z-axis. The first row (panels a, c and e) is for the on-axis incidence, while the second (panels b, d and f) for the off-axis with offset $(x_0, y_0) = (\pi/ka, 2\pi/ka)$. The left, middle, and right columns correspond to the rigid, total, and resonance scattering, respectively.

The fourth Rayleigh resonance ($ka = 13.38$) is suppressed with $\beta = 67.7923°$ for the root of $P_4^2(\cos\beta) = 0$, and the fifth Rayleigh resonance ($ka = 16.10$) is also suppressed with $\beta = 54.7356°$ for the root of $P_5^2(\cos\beta) = 0$. The nth resonance suppression will appear when the half-cone angle β is selected to make the corresponding term of $P_n^M(\cos\beta)$ (rather than $P_{n+M}^M(\cos\beta)$) vanish. For the on-axis incidence based on the plane-wave superposition method, the topological charge $M = m$ and the partial-wave series solution is independent of the azimuthal factor.

The 3-D patterns of the rigid background, the total, and resonance scattering for the FHBB at $ka = 10.46$ (the third-order Rayleigh resonance) are shown in Fig. 6 with the first row for the on-axis incidence and the second row for the off-axis case (offset is the same as that in Section IV). The half-cone angle is selected as $\beta = 63.4349°$ such that $P_3^1(\cos\beta) = 0$. The corresponding resonance suppressions are expected for both the on-axis and off-axis as shown in Fig. 6(e) and (f). However, the resonance scattering of the off-axis incidence is relatively stronger than that of the on-axis case. In addition, the rotational symmetry of the 3-D scattering patterns breaks since the incident Bessel beam is no longer axisymmetric relative to the sphere, as shown in Fig. 6(b), (d), and (f). For the off-axis incidence, the maximum form function modulus of the total scattering seemed to be smaller than that of the rigid background. This may be due to the destructive interference between the elastic waves and the impenetrable wave outside under this circumstance. Fig. 7 shows the 3-D scattering patterns with the same parameters as in Fig. 6, except that $\beta = 49.1066°$, which will not bring resonance suppression at $ka = 10.46$. The first row specifies the on-axis incidence, whereas the second is for the off-axis. An octupole mode of the resonance scattering could be observed in Fig. 7(e) for the on-axis incidence, with dips in the forward and backward directions ($\theta = 0°$ and $\theta = 180°$). Note that for the on-axis incidence by an OBB at $ka = 10.46$, the octupole mode has the peaks in the forward and backward directions (see [33, Fig. 7]). This may be due to the axial peak of the beam intensity for the OBB and the axial null for the HBBs in the propagation directions. Different from the case with $\beta = 63.4349°$ (where resonance suppression appears), the resonance scattering of the off-axis incidence is weaker than that of the on-axis incidence, as compared Fig. 7(e) with (f). The rotational symmetry vanishes under the off-axis illumination,

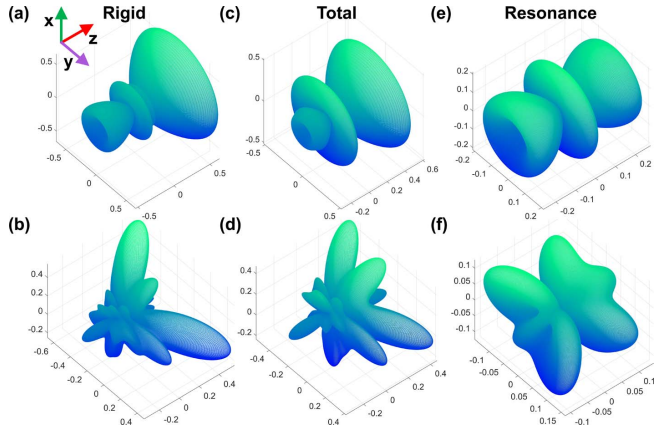

Fig. 7. Same as Fig. 6, except that $\beta = 49.1066°$ such that $P_3^1(\cos\beta) \neq 0$. The frequency of the third-order Rayleigh resonance is selected as $ka = 10.46$.

as shown in the second row in Fig. 7, which is due to the fact that the acoustic field is no longer symmetry with respect to the sphere although the beam itself and the sphere are axisymmetric with their own centers.

VI. Scattering From a Spherical Shell in a Helicoidal Bessel Beam

After the discussion of acoustic scattering from a solid sphere in both the OBB and HBB, the spherical shell will be briefly studied under the illumination of an HBB in this section. According to the RST, a rigid background should be subtracted from the total scattering to approximately extract out the pure resonance scattering contribution for a solid sphere. However, the rigid background is not always applicable to the shell case. In general, the soft background should be applied for a thin shell, while the rigid background should be used for a thick shell [15], [16], [24]–[26]. Under certain circumstances for the same object, the soft background is suitable at the lower frequency limit, while the rigid background is suitable at the higher frequency limit [28]. The aspect ratio of the inner radius to the outer radius from the transition of the thin to the thick shell is approximately $b/a = 0.975$ [15]. For a spherical shell with the immediate thickness, the hybrid model background [27], [28] may be used to isolate a more exact resonance contribution form the total scattering. In the present work, only the lower frequency limit is considered for the theoretical results so that the soft and rigid backgrounds could be applied for the thin and thick shells, respectively.

The considered shells are made of steel material with the density 7.84 g/cm^3. The transverse and longitudinal velocities in the steel are 3150 m/s and 5854 m/s, respectively. The ambient medium is water and the inner part of the spherical shell is empty. The total scattering of an empty thick shell from ordinary [4] and helicoidal [5] Bessel beams with the on-axis incidence were studied by Marston using the plane-wave superposition method based on the partial-wave series solution. By using another theoretical approach presented in the previous section, the resonance scattering of the spherical shell is isolated from the total field based on the RST. The present method could provide an analytical solution of the

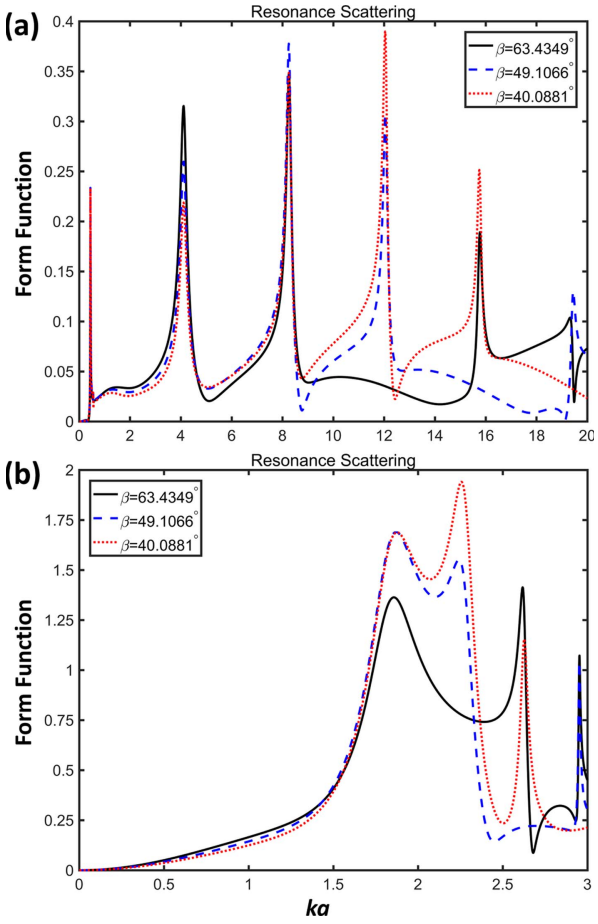

Fig. 8. Resonance scattering of the FHBB from a (a) thin and (b) thick empty steel shell at the scattering direction $\theta = 149.444°$ versus ka with the half-cone angles β selected for roots of $P_n^1(\cos\beta) = 0$.

off-axis incidence in the Bessel beam, as discussed for the sphere case above. A thin shell with the ratio of the inner-to-outer radii $b/a = 0.999$(thickness 0.1%) and thick shell with $b/a = 0.95$ (thickness 5%) are considered in the context of the FHBB with the on-axis incidence. Only the form function moduli versus dimensionless frequency of the pure resonance scattering are presented. The scattering angle θ is fixed at 149.444°. By subtracting a *soft background* for the thin shell and a *rigid background* for the thick shell, the form function moduli of pure resonance scattering are obtained as shown in Fig. 8(a) and (b). Like the results of a solid sphere, the explicit peaks corresponding to different resonant frequencies of certain order exhibit the suppression. For the thin shell in Fig. 8(a), the third to fifth resonances are at the dimensionless frequencies $ka = 12.04$, 15.75, and 19.44, respectively ($n = 3, 4$, and 5). The corresponding half-cone angles for the roots of $P_n^1(\cos\beta) = 0$ are $\beta = 63.4349°$, 49.4349°, and 40.0881° from $n = 3$ to 5 as listed in Table I. The resonance suppression appears at a certain order when β is selected to make $P_n^1(\cos\beta)$ vanish. Taking $\beta = 49.1066°$ such that $P_4^1(\cos\beta) = 0$, the fourth resonance at $ka = 15.75$ is greatly suppressed (the blue dashed line). In addition, the resonance form function modulus almost vanishes in the scattering direction ($\theta = 149.444°$) at

$ka = 19.13$. For the thick shell in Fig. 8(b), the third to fifth resonances occur at $ka = 2.256$, 2.618, and 2.952. Similarly, the resonance suppressions are observed when β is selected as the corresponding root of $P_n^1(\cos\beta) = 0$. The 3-D scattering patterns of the form function depict the similar phenomena for the on- and off-axis incidences as those of the solid sphere in Section V, which are not given here for simplicity. In addition, the 2-D pure resonance patterns of a thick shell were computed using the T-matrix in the zeroth-order OBB, which presented the suppression effects in the Bessel beam and gave the corresponding physical mechanism [33].

As observed in Fig. 8 for the thin and thick shells, the resonance peaks are relatively sharp and sparse for the thin shell compared with those of the thick shell. As explained in [34] for the plane wave case, for a thin shell, only the zeroth-order symmetric and antisymmetric Lamb modes dominate, whereas for the thick shell other modes play an active role including the external Franz waves, the waves scattered from the inner surface of the shell, and other types of Lamb waves. Note that the zeroth-order Lamb waves in the thin shell could propagate almost without dispersion. These could also apply for the Bessel beam illumination and explain the relatively simple structure of the resonance form function of a thin shell. The resonance peaks of the thin shell are almost equally spaced as shown in Fig. 8(a).

VII. Discussion and Conclusion

The present exact solution of acoustic scattering from a spherical shape of the Bessel beam based on the multipole expansion method [8], [13] gives a uniform and closed-form expression, which can be used for the OBBs and HBBs with the object located on or off the axis. This analytical method is a supplement to another theoretical method based on the plane wave superposition [3]–[5]. Meanwhile, the present work eliminates the singularity stemming from the term of $1/j_n(\mathrm{kb})$ in the beam-shape coefficients using the spherical harmonics transform, which both improves the accuracy and saves the computational cost. By using RST, the pure resonance scattering contribution is isolated from the total scattering for the solid sphere, the thin and thick shells, with the on-axis and off-axis incidences. Different from the ordinary plane waves, the Bessel beam may fail to induce the resonance of certain order with a special half-cone angle, which is explained with the physical mechanisms [4], [5] that the corresponding partial wave vanishes when the associated Legendre function is null in the series. The present results using the multipole expansion verified the resonance suppression for the on-axis case. In addition, consider an on-axis incident Bessel beam without resonance suppression, the resonance scattering patterns of the same object at the same frequency in an OBB [33, Fig. 7] are different from those of an HBB [Fig. 7(e)] since peaks occur in the forward and backward directions for OBB, while valleys come out for the HBB. This is due to the different intensity distributions of the OBBs and HBBs. However, the resonance modes are the same for both the OBB and HBB as the octupole mode at the third-order resonance, which is the intrinsic property of the elastic object and free of the incidence sources. Novel properties are found for resonance scattering under the off-axis incidence with the selected half-cone angle for roots of $P_n^m(\cos\beta) = 0$ at a corresponding resonance frequency. Under the same condition, except for an off-axis incidence, the resonance scattering seems to be relatively stronger than that of the on-axis incidence, as depicted in Figs. 3 and 6.

The present work provides another theoretical way to deal with the Bessel beam scattering with arbitrary topological charge and location for the spherical shapes as long as the scattering coefficients s_n are available, which provides a closed-form expression for both objects located at an arbitrary location to the beam center. The general expression of the beam shape coefficients of Bessel beams has been given in an integrated form before [11], [12], [35], which may still need further numerical computation. The incident beam-shape coefficient in (4) may be extended for a nonspherical object with the implementation of the T-matrix method [8], [22]–[24] and other numerical methods. There may be a transfer of the linear or angular momenta during the interaction of the acoustic fields of Bessel beams and targets. Based on the radiation stress tensor approach [36], the acoustic radiation force from a spherical shape centered on the axis [37]–[39] or at arbitrary location [40]–[42] of Bessel beams could be calculated in terms of real and imaginary parts of the scattering coefficients, where negative radiation forces are found under certain circumstances. In addition, a radiation force expression based on the radiation stress tensor approach was derived based on the far-field approximation of the spherical Bessel/Hankel functions and the related recursion in terms of the incident and scattered beam-shape functions [42], [43], which could be solved for Bessel beams of arbitrary order and location using the partial-wave series solution and the T-matrix method. Note that the main focus for acoustic manipulation lies on the small particles recently which will use the Gor'kov potential for simplicity and efficiency. However, the larger particle is still challenging in the acoustofluidics in the aspect of experiments or applications, so it is promising to apply the resonance effect for controlling large particles with the size comparable to the wavelength. The resonance effect related to the acoustic radiation force has been studied recently for the spherical [44] and cylindrical shapes [45], [46]. Furthermore, the present work could be further extended for the study of acoustic radiation torque in Bessel beams [43], [47].

References

[1] J. Durnin, "Exact solutions for nondiffracting beams. I. The scalar theory," *J. Opt. Soc. Amer. A, Opt. Image Sci.*, vol. 4, no. 4, pp. 651–654, 1987.

[2] J. Durnin, J. J. Miceli, and J. H. Eberly, "Diffraction-free beams," *Phys. Rev. Lett.*, vol. 58, no. 15, p. 1499, 1987.

[3] P. L. Marston, "Scattering of a Bessel beam by a sphere," *J. Acoust. Soc. Amer.*, vol. 121, no. 2, pp. 753–758, 2007.

[4] P. L. Marston, "Acoustic beam scattering and excitation of sphere resonance: Bessel beam example," *J. Acoust. Soc. Amer.*, vol. 122, no. 1, pp. 247–252, 2007.

[5] P. L. Marston, "Scattering of a Bessel beam by a sphere: II. Helicoidal case and spherical shell example," *J. Acoust. Soc. Amer.*, vol. 124, no. 5, pp. 2905–2910, 2008.

[6] F. G. Mitri, "Acoustic scattering of a high-order Bessel beam by an elastic sphere," *Ann. Phys.*, vol. 323, no. 11, pp. 2840–2850, 2008.

[7] F. G. Mitri, "Equivalence of expressions for the acoustic scattering of a progressive high-order Bessel beam by an elastic sphere," *IEEE Trans. Ultrason., Ferroelectr., Freq. Control*, vol. 56, no. 5, pp. 1100–1103, May 2009.

[8] Z. Gong, P. L. Marston, W. Li, and Y. Chai, "Multipole expansion of acoustical Bessel beams with arbitrary order and location," *J. Acoust. Soc. Amer.*, vol. 141, no. 6, pp. EL574–EL578, 2017.

[9] Z. Xu, W. Xu, M. Qian, Q. Cheng, and X. Liu, "A flat acoustic lens to generate a Bessel-like beam," *Ultrasonics*, vol. 80, pp. 66–71, Sep. 2017.

[10] R. D. Muelas-Hurtado, J. L. Ealo, J. F. Pazos-Ospina, and K. Volke-Sepulveda, "Generation of multiple vortex beam by means of active diffraction gratings," *Appl. Phys. Lett.*, vol. 112, no. 8, Feb. 2018, Art. no. 084101. doi: 10.1063/1.5016864.

[11] G. T. Silva, "Off-axis scattering of an ultrasound Bessel beam by a sphere," *IEEE Trans. Ultrason., Ferroelectr., Freq. Control*, vol. 58, no. 2, pp. 298–304, Feb. 2011.

[12] F. G. Mitri and G. T. Silva, "Off-axial acoustic scattering of a high-order Bessel vortex beam by a rigid sphere," *Wave Motion*, vol. 48, no. 5, pp. 392–400, 2011.

[13] J. J. Wang, T. Wriedt, L. Mädler, Y. P. Han, and P. Hartmann, "Multipole expansion of circularly symmetric Bessel beams of arbitrary order for scattering calculations," *Opt. Commun.*, vol. 387, pp. 102–109, Mar. 2017.

[14] L. Zhang, "A general theory of arbitrary Bessel beam scattering and interactions with a sphere," *J. Acoust. Soc. Amer.*, vol. 143, no. 5, pp. 2796–2800, 2018.

[15] L. Flax, G. C. Gaunaurd, and H. Überall, "Theory of resonance scattering," *Phys. Acoust.*, vol. 15, pp. 191–294, Jan. 1981.

[16] L. Flax, L. R. Dragonette, and H. Überall, "Theory of elastic resonance excitation by sound scattering," *J. Acoust. Soc. Amer.*, vol. 63, no. 3, pp. 723–731, 1978.

[17] J. D. Jackson, *Classical Electrodynamics*, 3rd ed. New York, NY, USA: Wiley, 1999, Secs. 3.5-3.6, pp. 107–111.

[18] L. I. Schiff, *Quantum Mechanics*, 3rd ed. New York, NY, USA: McGraw-Hill, 1968, pp. 131–133.

[19] P. C. Waterman, "New formulation of acoustic scattering," *J. Acoust. Soc. Amer.*, vol. 45, no. 6, pp. 1417–1429, 1969.

[20] V. V. Varadan, A. Lakhtakia, and V. K. Varadan, *Field Representations and Introduction to Scattering*. Amsterdam, The Netherlands: Elsevier, 1991, Sec. 5.1, pp. 234–239.

[21] W. G. Neubauer, R. H. Vogt, and L. R. Dragonette, "Acoustic reflection from elastic spheres. I. Steady-state signals," *J. Acoust. Soc. Amer.*, vol. 55, no. 6, pp. 1123–1129, 1974.

[22] W. Li, Y. Chai, Z. Gong, and P. L. Marston, "Analysis of forward scattering of an acoustical zeroth-order Bessel beam from rigid complicated (aspherical) structures," *J. Quant. Spectrosc. Radiat. Transf.*, vol. 200, pp. 146–162, Oct. 2017.

[23] Z. Gong, W. Li, F. G. Mitri, Y. Chai, and Y. Zhao, "Arbitrary scattering of an acoustical Bessel beam by a rigid spheroid with large aspect-ratio," *J. Sound Vibr.*, vol. 383, pp. 233–247, Nov. 2016.

[24] M. F. Werby, H. Überall, A. Nagl, S. H. Brown, and J. W. Dickey, "Bistatic scattering and identification of the resonances of elastic spheroids," *J. Acoust. Soc. Amer.*, vol. 84, no. 4, pp. 1425–1436, 1988.

[25] J. D. Murphy, J. George, A. Nagl, and H. Überall, "Isolation of the resonant component in acoustic scattering from fluid-loaded elastic spherical shells," *J. Acoust. Soc. Amer.*, vol. 65, no. 2, pp. 368–373, 1979.

[26] M. F. Werby and L. H. Green, "A comparison of acoustical scattering from fluid-loaded elastic shells and sound soft objects," *J. Acoust. Soc. Amer.*, vol. 76, no. 4, pp. 1227–1230, 1984.

[27] G. C. Gaunaurd and M. F. Werby, "Sound scattering by resonantly excited, fluid-loaded, elastic spherical shells," *J. Acoust. Soc. Amer.*, vol. 90, no. 5, pp. 2536–2550, 1991.

[28] M. F. Werby, "The acoustical background for a submerged elastic shell," *J. Acoust. Soc. Amer.*, vol. 90, no. 6, pp. 3279–3287, 1991.

[29] S. M. Hasheminejad and M. Rajabi, "Acoustic resonance scattering from a submerged functionally graded cylindrical shell," *J. Sound Vibr.*, vol. 302, nos. 1–2, pp. 208–228, 2007.

[30] M. Rajabi and S. M. Hasheminejad, "Acoustic resonance scattering from a multilayered cylindrical shell with imperfect bonding," *Ultrasonics*, vol. 49, no. 8, pp. 682–695, 2009.

[31] P. L. Marston, "Generalized optical theorem for scatterers having inversion symmetry: Applications to acoustic backscattering," *J. Acoust. Soc. Amer.*, vol. 109, no. 4, pp. 1291–1295, 2001.

[32] P. L. Marston, "Quantitative ray methods for scattering," in *Encyclopedia of Acoustics*, M. J. Crocker, Ed. New York, NY, USA: Wiley, 1997, ch. 43, pp. 483–492.

[33] S. Liu, Z. Gong, Y. Chai, and W. Li, "Underwater acoustic scattering of Bessel beam by spherical shell using T-matrix method," in *Proc. IEEE/OES China Ocean Acoust.*, Harbin, China, Jan. 2016, pp. 1–6.

[34] G. C. Gaunaurd and M. F. Werby, "Lamb and creeping waves around submerged spherical shells resonantly excited by sound scattering," *J. Acoust. Soc. Amer.*, vol. 82, no. 6, pp. 2021–2033, 1987.

[35] F. G. Mitri, "Generalized theory of resonance scattering (GTRS) using the translational addition theorem for spherical wave functions," *IEEE Trans. Ultrason., Ferroelectr., Freq. Control*, vol. 61, no. 11, pp. 1880–1888, Nov. 2014.

[36] C. P. Lee and T. G. Wang, "Acoustic radiation pressure," *J. Acoust. Soc. Amer.*, vol. 29, no. 1, pp. 26–29, 1957.

[37] P. L. Marston, "Axial radiation force of a Bessel beam on a sphere and direction reversal of the force," *J. Acoust. Soc. Amer.*, vol. 120, no. 6, pp. 3518–3524, 2006.

[38] P. L. Marston, "Negative axial radiation forces on solid spheres and shells in a Bessel beam," *J. Acoust. Soc. Amer.*, vol. 122, no. 6, pp. 3162–3165, 2007.

[39] P. L. Marston, "Radiation force of a helicoidal Bessel beam on a sphere," *J. Acoust. Soc. Amer.*, vol. 125, pp. 3539–3547, Jun. 2009.

[40] G. T. Silva, J. H. Lopes, and F. G. Mitri, "Off-axial acoustic radiation force of repulsor and tractor Bessel beams on a sphere," *IEEE Trans. Ultrason., Ferroelectr., Freq. Control*, vol. 60, no. 6, pp. 1207–1212, Jun. 2013.

[41] F. G. Mitri, "Acoustics of finite asymmetric exotic beams: Examples of Airy and fractional Bessel beams," *J. Appl. Phys.*, vol. 122, no. 22, Dec. 2017, Art. no. 224903.

[42] Z. Gong, P. L. Marston, and W. Li. (2017). "T-matrix evaluation of acoustic radiation forces on nonspherical objects in Bessel beams." [Online]. Available: https://arxiv.org/abs/1710.00146

[43] Z. Gong, "Study on acoustic scattering characteristics of objects in Bessel beams and the related radiation force and torque," (in Chinese), Ph.D. dissertation, School Naval Archit. Ocean Eng., Huazhong Univ. Sci. Technol., Wuhan, China, 2018.

[44] M. Rajabi and A. Mojahed, "Acoustic manipulation: Bessel beams and active carriers," *Phys. Rev. E, Stat. Phys. Plasmas Fluids Relat. Interdiscip. Top.*, vol. 96, Oct. 2017, Art. no. 043001.

[45] M. Rajabi and M. Behzad, "On the contribution of circumferential resonance modes in acoustic radiation force experienced by cylindrical shells," *J. Sound Vibr.*, vol. 333, no. 22, pp. 5746–5761, 2014.

[46] M. Rajabi and M. Behzad, "An exploration in acoustic radiation force experienced by cylindrical shells via resonance scattering theory," *Ultrasonics*, vol. 54, no. 4, pp. 971–980, 2014.

[47] L. Zhang and P. L. Marston, "Angular momentum flux of nonparaxial acoustic vortex beams and torques on axisymmetric objects," *Phys. Rev. E, Stat. Phys. Plasmas Fluids Relat. Interdiscip. Top.*, vol. 84, no. 6, Dec. 2011, Art. no. 065601.